Polymer Chemistry

ROYAL SOCIETY OF CHEMISTRY

PAPER

View Article Online
View Journal | View Issue

Cite this: *Polym. Chem.*, 2023, **14**, 201

Model dynamic covalent thermoresponsive amphiphilic polymer co-networks based on acylhydrazone end-linked Tetronic T904 star block copolymers†

Demetris E. Apostolides,[a] Costas S. Patrickios, *[a] Miriam Simon,[b] Michael Gradzielski, [b] Adam Blanazs, [c] Cécile Mussault,[d] Alba Marcellan,[d,e] Nicolas Alexander[f] and Chrys Wesdemiotis[f]

Self-healable, reversible, recyclable, stretchable, thermoresponsive and self-assembled model amphiphilic polymer co-networks (APCNs) were prepared by end-linking Tetronic T904 amphiphilic four-armed star block copolymers of poly(ethylene glycol) (PEG, peripheral blocks) and poly(propylene glycol) (PPG, internal blocks) *via* dynamic covalent acylhydrazone bonds. These newly developed APCNs were first explored in terms of their dynamic covalent properties, including self-healing, recyclability and reversibility. Remarkably, for the last property, it was possible to determine the percentage of acylhydrazone cross-links for each of the several sol–gel transition cycles, both in the gel (originally formed and reformed APCNs) and solution (dissociated APCNs) states using simple solution (rather than magic angle spinning) ^{1}H NMR spectroscopy. The recorded ^{1}H NMR spectra indicated that the acylhydrazone percentage in the gel state monotonically declined from 92% in the first cycle down to 70% in the seventh cycle, whereas the corresponding percentage in the solution state monotonically increased from 20% up to 55% in the first and sixth cycles, respectively. An additional ^{1}H NMR spectroscopy study based on a model reaction using monofunctionalized PEGs indicated that this incomplete reversibility originates from the slowing down of the reformation reaction from the fifth cycle onwards, with new signals from the benzaldehyde end-group being observable in the seventh cycle probably arising from the "salting out" of the benzaldehyde group in the environment of increased triethylamine hydrochloride concentration. Subsequently, the prepared APCNs were characterized in terms of their self-assembly behavior using small-angle neutron scattering (SANS) in D_2O. SANS indicated APCN microphase separation when the temperature was raised from room temperature to 40–50 °C, with the formation of rather small spherical micellar domains (aggregation numbers of ~8.5 T904 units) with hydrated hydrophobic cores with radii of 3 nm, located within larger domains of ~50 nm radii. These APCNs are thermoresponsive materials where the increasing temperature leads to an increased structural organization and improved tensile mechanical properties, particularly the stress at break and Young's modulus, which were enhanced by 160% and 130%, respectively.

Received 3rd October 2022,
Accepted 23rd November 2022

DOI: 10.1039/d2py01256a

rsc.li/polymers

[a]*Department of Chemistry, University of Cyprus, P. O. Box 20537, 1678 Nicosia, Cyprus. E-mail: apostolides.demetris@ucy.ac.cy, costasp@ucy.ac.cy; Tel: (+357) 22 892768*

[b]*Stranski-Laboratorium für Physikalische und Theoretische Chemie, Institut für Chemie, Straße des 17. Juni 124, Technische Universität Berlin, D-10623 Berlin, Germany. E-mail: miriam.simon@campus.technion.ac.il, michael.gradzielski@tu-berlin.de*

[c]*BASF SE, GMV/P – B001, D67056 Ludwigshafen am Rhein, Germany. E-mail: adam.blanazs@basf.com*

[d]*Sciences et Ingénierie de la Matière Molle, ESPCI Paris, PSL University, Sorbonne University, CNRS, F-75005 Paris, France. E-mail: cecile.mussault@espci.fr*

[e]*Institut Universitaire de France, Paris, France. E-mail: alba.marcellan@espci.psl.eu*

[f]*Department of Chemistry and Integrated Biosciences Program, University of Akron, Akron, Ohio 44325-3601, USA. E-mail: nea16@zips.uakron.edu, wesdemi@uakron.edu*

†Electronic supplementary information (ESI) available: Experimental part with information on synthesis (end-functionalizations) and characterization, and extra results with the reaction scheme of the end-functionalizations of the T904 star block copolymer. The ^{1}H NMR spectra, GPC and MALDI-TOF, and calculated molar masses of the starting T904 (T904-OH), intermediate (T904-MS and T904-PRHz) and final (T904-Bz and T904-Hz) end-functionalization products. The ^{1}H NMR spectra of the starting PEG-OH 550, intermediate (PEG-MS and PEG-PRHz) and final (PEG-Bz and PEG-Hz) end-functionalization products. The ^{1}H NMR spectra of the reformed acylhydrazone adduct after the first and seventh cycles, the ^{1}H NMR spectra of PEG-Bz after the first and seventh DCl-triethylamine addition, the ATR-FTIR spectra of dried APCN gel and its precursors, rheology on gel formation and rheological frequency sweeps, compressive mechanical properties, the SANS model, data fits and related parameters, and the temperature dependence of the aqueous degree of swelling. See DOI: https://doi.org/10.1039/d2py01256a

Introduction

Polymeric hydrogels are important materials uniquely combining an aqueous fluid nature with an elastic network structure, thereby allowing the diffusive transport of solutes while maintaining a solid texture. Amphiphilic polymer co-networks (APCN), representing a particular type of polymeric hydrogels, possess, in addition to the hydrophilic units, sequences of hydrophobic units, enabling swelling also in non-polar organic solvents ("oils"), and reducing the swelling in aqueous media.[1,2] Most important, however, is their structural organization in aqueous media, a result of the concealment of the hydrophobic sequences in non-polar pockets. The non-polar pockets can host sizeable quantities of hydrophobic solutes, either to be delivered, *e.g.*, hydrophobic drug delivery,[3] or, conversely, to be transported from the external aqueous milieu into the APCNs, *e.g.*, sequestration of hydrophobic environmental pollutants.[4] Finally, the formed hydrophobic domains mechanically reinforce[5–7] the APCNs, as their reversible deformation provides another energy dissipation mechanism. These enhanced mechanical properties and the internal self-assembly of APCNs are important for their applications, which, in addition to the above-mentioned drug delivery, also include the fabrication of soft contact lenses (the most successful APCN application with global annual sales of 10 billion US dollars),[8] and emerging applications in energy[9–13] and analytical science.[14] A new exciting prospect is the employment of APCNs (in the form of soft contact lenses) for ocular drug delivery.[15] Recent related works have also involved porous networks[16–19] with applications in iodine adsorption, chiral separations, self-sorting, adhesion, and even forming optically active semiconducting nanofibers.[20–22]

In addition to amphiphilicity, two other important and timely attributes in polymer networks are well-defined structures and dynamic covalent cross-linking.[23] Dynamic covalent cross-links secure the self-healing, reversibility and recyclability of polymer networks,[24–26] whereas the well-defined (near-perfect or model) structure arises from polymer chain length homogeneity, again leads to better mechanical properties, and, upon characterization, it enables the derivation of accurate structure–property relationships.[27] Although amphiphilicity, dynamic covalent nature and near perfect structures have only been addressed in the literature separately or in pairs, the combination of all three attributes together can rarely be found in a single investigation.[28] In the only study combining all three attributes together, structural characterization was not performed. Thus, the aim of this study is to design, prepare and fully characterize model APCNs cross-linked *via* dynamic covalent bonds. Our findings include important insights into the conversion to the acylhydrazone dynamic covalent cross-links upon each of the several consecutive gel–sol–gel cycles, and the effect of temperature on the self-assembly and mechanical properties of the APCN.

Experimental section

For experimental details, see the ESI.†

Results and discussion

Aqueous formation of the dynamic covalent APCNs

Fig. 1 illustrates the formation of the dynamic covalent APCNs in this study. APCN formation results from the end-linking of two types of amphiphilic four-armed star block copolymers, differing only in their end-groups, benzaldehyde and benzaacylhydrazide, whose reactions lead to the formation of bisaryl-substituted acylhydrazone groups serving as dynamic covalent cross-links. The chosen four-armed amphiphilic star block copolymer comprised poly(ethylene glycol) (PEG) peripheral blocks and poly(propylene glycol) (PPG) internal blocks, with a rather high content of the more hydrophobic PPG component (approximately 16 monomer repeating units in each of the two block types, PEG and PPG, per arm), so as to provide a large driving force for self-assembly, but without compromising room temperature water-solubility. The particular star block copolymer was the commercially available Tetronic T904, originally bearing four hydroxyl end groups. These hydroxyl groups were modified to the two types of the above-mentioned end-groups by following our previous work on four-armed PEG star homopolymer (tetraPEG) dynamic covalent gels (tetraPEG

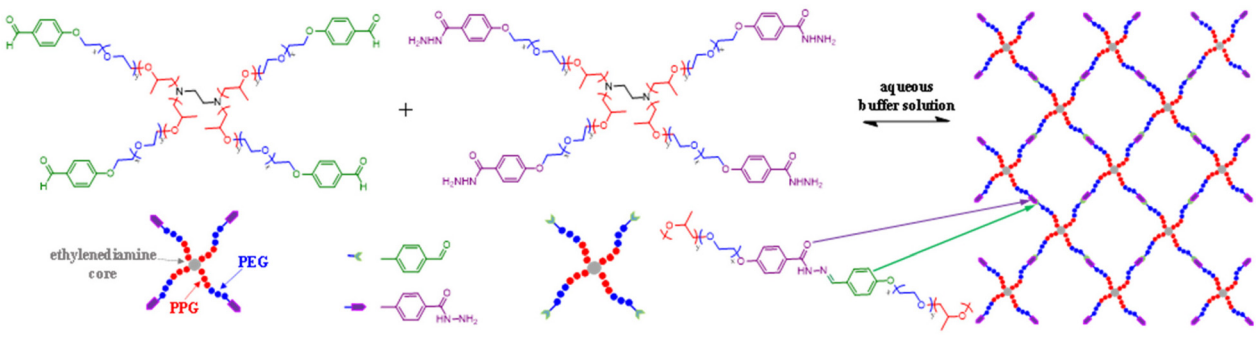

Fig. 1 Formation of the dynamic covalent APCNs *via* the acylhydrazone end-linking of the two types of T904 Tetronics, with *x* and *y* being equal to about 16.

DYNAgels),[29] which was based on the work of Deng *et al.*[30] improved to be applicable for higher molar mass polymers.[29] The experimental procedure for the end-group modification was that reported in our previous work,[29] while the modification scheme, the ^{1}H NMR and MALDI-TOF spectra, and the gel permeation chromatograms of the starting, intermediate and final products, and the calculated molar masses are provided in Fig. S1–S5 and Table S1 in the ESI.†

The dynamic covalent T904 APCNs were formed upon mixing equimolar acidic aqueous buffer solutions of the two complementarily end-functionalized amphiphilic star block copolymers, as illustrated in Fig. 1. Gels were typically prepared at a polymer concentration of 15% w/v in a 200 mM aqueous acetate buffer of pH 5.5, but they could also be formed at polymer concentrations down to 5% w/v, and in aqueous buffers up to pH 6.0. The higher pH limit was imposed by the room temperature aqueous solubility of the two types of more hydrophobic T904 amphiphilic star block copolymers, the benzaldehyde-derivatized one (T904-Bz), owing to its solubility at pH $\leq$ 6.0 to the ionization of the two nitrogen atoms in its ethylenediamine core. The pH-dependence of APCN formation times, determined using both tube inversion (gelation criterion was inability to flow) and rheology (gel formation time was taken as the moment when the shear elastic modulus, G', exceeded the shear loss modulus, G'', see Fig. S6†) experiments are plotted in Fig. 2. The gel formation times from the two techniques were close to each other, and increased almost linearly in the semi-logarithmic plot from 1 min at pH 2.0 to 100 min at pH 5.5. The exponential increase in the gel formation times with increasing pH is due to the exponential reduction in the concentration of the hydrogen ions catalyzing the formation of the acylhydrazone cross-links.[31]

Self-healing, reversibility and recyclability of the APCNs

The dynamic covalent properties of the developed APCNs were explored using several tests, both qualitative and quantitative. Two qualitative and three quantitative tests were performed and are illustrated in Fig. 3. The first qualitative test was self-healing (part (a) of the figure) in which two gel pieces, cut from two different gel samples (one dyed with malachite green) both formed by mixing pairs of aqueous polymer solutions buffered at pH 2.0, could adhere well to each other after pressing them together. The second qualitative test involved gel–sol–gel transitions (part (b) in the figure), where gel prepared in pure water with added glacial acetic acid could be dissolved by the addition of strong acid, HCl, and reformed by the addition of an equivalent amount of triethylamine (TEA) base, where this gel–sol–gel cycle could be repeated a few times before insoluble salt formation and dilution effects inhibited gel reformation (also see following section on the Origin of Incomplete Gel Reversibility).

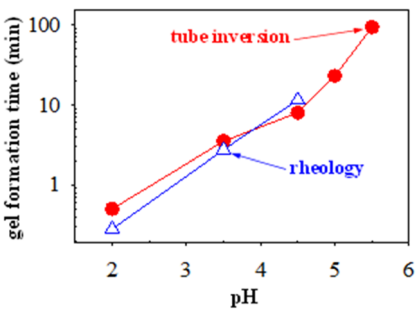

Fig. 2 Dependence of the dynamic covalent T904 APCN formation time on the pH of the aqueous buffer solution, determined using rheology and tube inversion experiments.

The next three quantitative tests aimed at evaluating the dynamic covalent properties of the APCNs. The first two were similar to the second qualitative test, which also involved gel dissolution and reformation, whereas the third quantitative test explored the cross-link lifetime in APCNs under conditions favoring the fast exchange of the acylhydrazone bond. The first quantitative test was performed by simple solution (rather than magic angle spinning) ^{1}H NMR spectroscopy to determine the yields of acylhydrazone bond formation, dissociation and reformation in APCNs originally formed in D_2O with added glacial acetic acid. At this point, we wish to stress that the herein recorded solution ^{1}H NMR spectra constitute *a rare example*[23,32] *of such spectra obtained for cross-linked APCNs* and represent one novelty in this study. Despite their semi-solid nature, the present APCNs exhibited clear and rather narrow peaks in their ^{1}H NMR spectra, possibly as a result of the modest hydrophobicity of the PG units and their constantly exchanging cross-links (see also their third quantitative characterization test below). Thus, cross-links formed in APCNs with more hydrophobic components might not be easily resolved by ^{1}H NMR spectroscopy as in the present system with the marginally hydrophobic PPG segments.

For this first quantitative test, APCN dissolution and reformation were performed in an NMR tube, where the original gel was also formed and from which all ^{1}H NMR spectra were recorded. After the ^{1}H NMR spectrum of the originally formed APCN in the NMR tube was recorded, the APCN was dissolved *via* the addition of a small volume of concentrated DCl solution in D_2O within the NMR tube (DCl molar loading was 10 times the number of moles of acylhydrazide groups initially loaded in the system), and the dissolution products were analyzed again by ^{1}H NMR spectroscopy (Fig. 4). The gel was subsequently reformed *via* the addition of a stoichiometric amount of TEA to the added DCl, and the gel was reanalyzed by ^{1}H NMR spectroscopy. This was repeated until the gel could not be reformed upon TEA addition, which occurred on cycle number 7. The percentage of acylhydrazone bonds relative to the aldehyde protons of the initial benzaldehyde was calculated from the spectra of all samples, both gels and solutions. These results are plotted in part (c) of Fig. 3.

Fig. 3(c) shows that, while the percentage of acylhydrazone bonds in the original gel was very high, above 90% (also consistent with the results from FTIR spectroscopy given in Fig. S7†), this percentage gradually declined down to about 65% at the sixth cycle. On the other hand, the percentage of acylhydrazone bonds present in the products in the first dis-

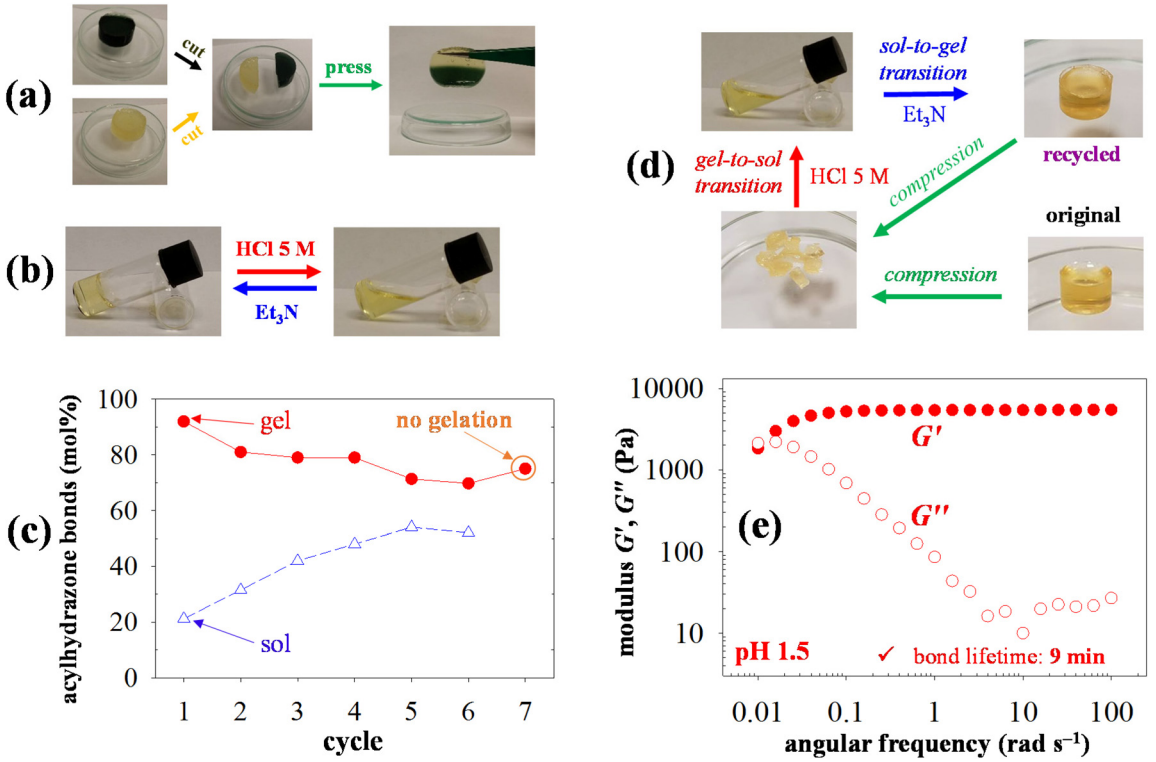

Fig. 3 Exploration of the dynamic covalent properties of the T904 APCNs developed in this study. (a) Self-healing of APCNs formed from pairs of aqueous polymer solutions. (b) APCN reversibility effected by their consecutive dissolution and reformation *via* the addition of acid and base, respectively. (c) Percentage of acylhydrazone cross-links in APCN gels and their solutions obtained in seven cycles of dissolution and reformation as determined by ^{1}H NMR spectroscopy. (d) Evaluation of compressive mechanical properties of virgin and recycled APCNs. (e) Rheological frequency sweep experiments for the determination of the lifetimes of the acylhydrazone cross-links. Parts (a) and (e): APCNs formed in 0.2 M phosphoric acid buffers at pH 2.0 (a) and 1.5 (e). Parts (b–d): APCNs formed in pure water (b and d) or D_2O (c) with the addition of a small volume (~2 μL) of glacial acetic acid.

solution cycle was about 20% (rather than 0%, also see the following section describing the reactions using model monofunctional PEG compounds), but that number gradually increased up to 50% with the increase in the cycle number. Thus, the percentage of acylhydrazone bonds in the gels decreases with the number of reformation cycles, while the corresponding percentage in the dissolved sample increases, with the two numbers converging. Eventually, in the seventh cycle, the gel could not be reformed. This incomplete reversibility has to be attributed to a combination of factors, including gradual functional group degradation, dilution effects and triethylamine hydrochloride salt formation at each cycle, finite concentrations of acid and base added, and the finite periods of time allowed between consecutive gel dissolution and reformation steps. Yet, it is remarkable that the signals from the acylhydrazone cross-links were clearly visible in the ^{1}H NMR spectra of both the gels and solutions and the percentages of those cross-links were expectedly higher in the gels than in the solutions, with the percentages in the two systems converging, explaining the eventual inability for gel reformation on the seventh cycle.

The second and third quantitative tests concerned the mechanical properties of reformed APCNs (Fig. 2(d)) and the cross-link lifetime in acidic APCNs (Fig. 3(e)), respectively. Regarding the former, mechanical testing indicated that the compressive Young's modulus and compressive stress and strain at break of original ("virgin") and reformed ("recycled") APCNs were the same, within experimental error (Table S2†). Regarding the latter, rheological frequency sweep experiments yielded cross-link lifetimes of 9 and 39 min for APCNs formed in 200 mM aqueous buffers of pH 1.5 and 2.0 (Fig. S8†), respectively. More discussion on these two quantitative tests is provided in the ESI.†

Origin of incomplete gel reversibility

Next, we pursued the elucidation of the origin of incomplete gel reversibility. The incomplete reversibility of acylhydrazone-linked gels was first pointed out by Deng and co-workers in their seminal study,[30] where, in addition to gel clouding, these investigators also observed a downgrading of the rheological properties of the gels upon their repeated dissociation and reformation. Our chosen approach involved the study of a model acylhydrazone formation reaction between two monofunctionalized, rather than tetrafunctionalized, PEG-OHs, one with benzaldehyde, PEG-Bz, and the other with acylhydrazide (PEG-Hz). PEG-OH with a molar mass of 550 g mol^{-1} (PEG-OH

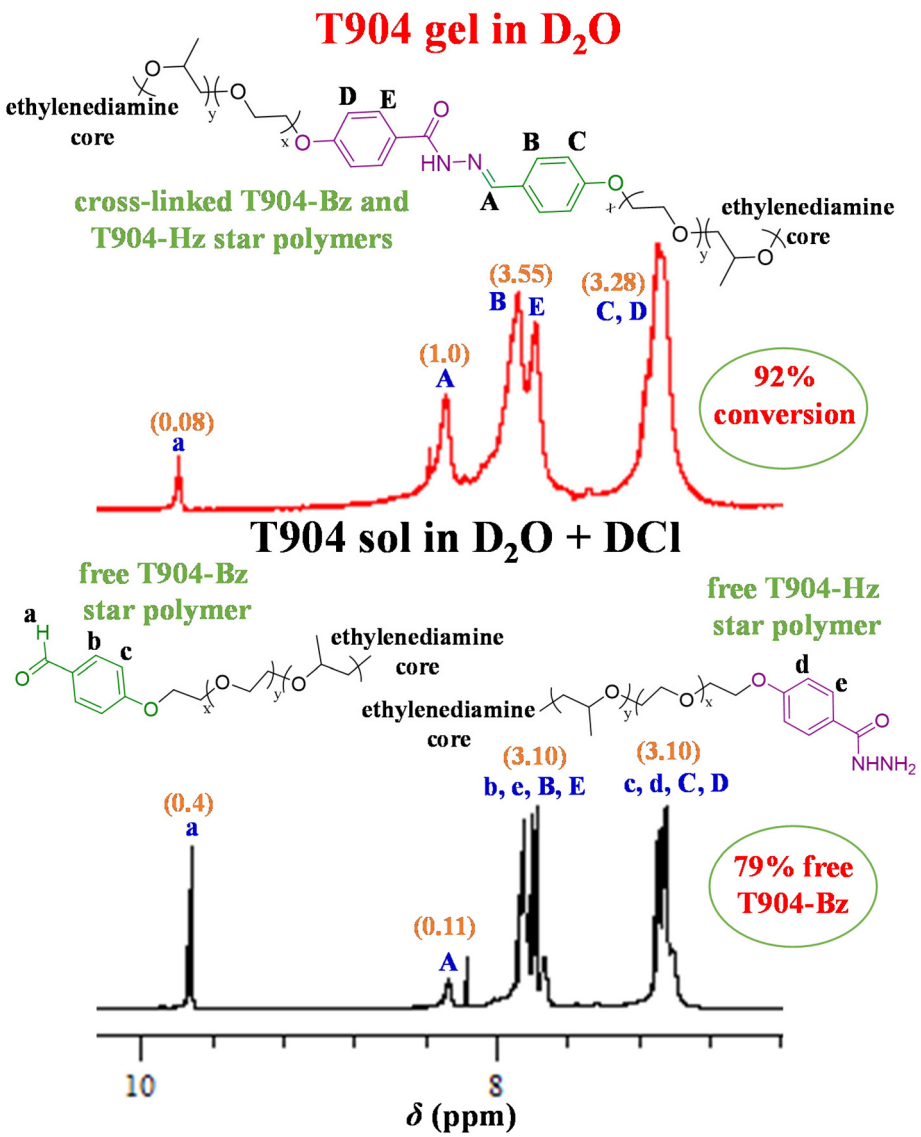

Fig. 4 Simple solution ^{1}H NMR spectra in D_2O of the originally formed APCN gel (top), and the same sample after its dissolution *via* the addition of DCl in D_2O (bottom). The sharp singlet at 8.20 ppm is due to traces of DMF.

550) was employed, which was end-functionalized to obtain the two derivatives using similar synthetic routes to those utilized for Tetronic T904. The information on the synthesis and characterization of PEG-Bz and PEG-Hz are provided in the ESI (^{1}H NMR spectra are illustrated in Fig. S9 and S10†). The experiments were performed under the same conditions as gel formation and dissociation with the Tetronic T904 star block copolymers, *i.e.*, in neat D_2O with the addition of a catalytic amount of 2 μL glacial acetic acid, and the same initial concentration of 55 mmol of benzaldehyde and acylhydrazide functional groups. However, unlike the experiments with the tetrafunctional star compounds giving gels, the present experiments with the monofunctional compounds were much faster both in dissociation (addition of DCl) and association (addition of triethylamine) and did not exhibit any obvious turbidity arising from the triethylamine hydrochloride salt formed at the end of each cycle. The present reversibility experiment was also performed for seven cycles, but the kinetics of the dissociation and association reactions was now carefully followed by ^{1}H NMR spectroscopy to make sure that enough time was allowed for the reactions to reach completion.

The collected data for all seven cycles are presented in two different ways in parts (a) and (b) of Fig. 5. Part (a) of the figure illustrates the temporal evolution of acylhydrazone bond concentration expressed as the percentage of the maximum amount of acylhydrazone bonds that can be formed, based on the stoichiometric amounts of benzaldehyde and acylhydrazide, added to the system. Each cycle first involves DCl addition (5-fold with respect to the initial molar amount of acylhydrazide or benzaldehyde groups present), followed by the addition of a stoichiometric (relative to DCl) amount of triethylamine. One can see from this part of the figure that, for

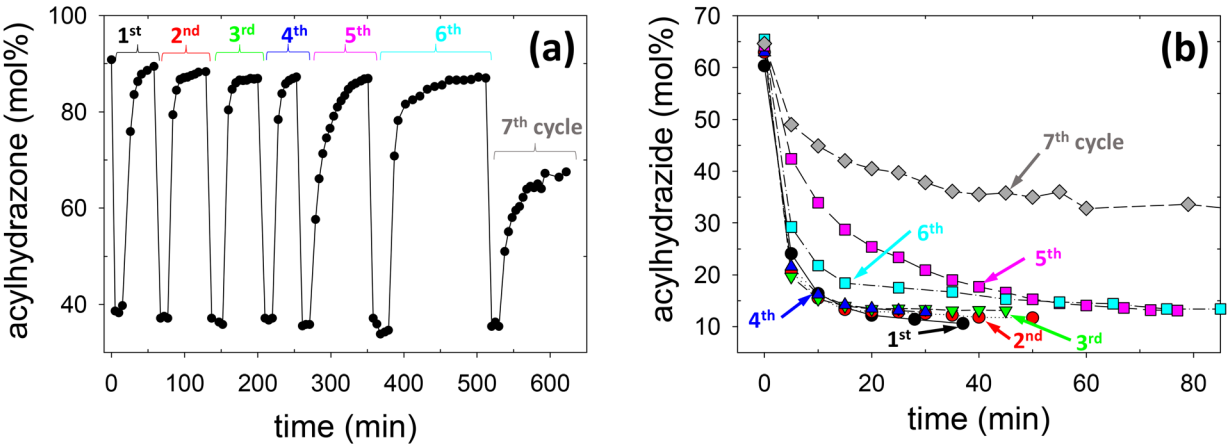

Fig. 5 (a) Temporal evolution of the dissociation (addition using a 5-fold DCl amount) and association (addition of equivalent amount of triethylamine to neutralize DCl) of a model, water-soluble acylhydrazone compound over seven cycles. (b) Overlay of only the acylhydrazone reformation (association) parts (the beginning of each curve was shifted to time zero), in the form of reduction in the acylhydrazide concentration.

all seven cycles, DCl addition leads to a rapid reduction of the acylhydrazone concentration from about 90% down to about 40% of its maximum theoretical concentration, followed by a slower recovery of acylhydrazone concentration upon the addition of a stoichiometric (relative to DCl) amount of triethylamine, back to about 90%, except for cycle number seven, for which recovery is only about one half of the recovery observed in the previous cycles.

In order to also gain an understanding of the kinetics of acylhydrazone bond recovery, especially in the later cycles, the data in part (a) are replotted in part (b), where all acylhydrazone bond recovery kinetics are overlaid by starting all recovery branches at time zero, omitting all dissociation branches. Here, however, the acylhydrazide concentration, rather than acylhydrazone, (again as a percentage) is plotted instead. Fig. 5(b) clearly shows that the reduction in acylhydrazide concentration is equally fast in the first four reassociation cycles (which are almost indistinguishable from each other), and becomes slower in the last three cycles. Although the reassociation is slower in cycles five and six, the conversions of the reaction reach those attained in the previous cycles; it is in cycle seven that the reaction is both slower and fails to reach the high conversions attained in the other cycles, as already observed from Fig. 5(a). Inspecting all the ^{1}H NMR spectra, we observed that the peak due to the benzaldehyde formyl methine proton at 9.8 ppm was split into two in all the spectra of cycle number seven (Fig. S11†). Thus, benzaldehyde degradation/modification might be the origin of acylhydrazone incomplete reversibility. We examined this hypothesis by "aging" PEG-Bz in the presence of 5-fold molar amounts of DCl or triethylamine for five days. However, for this timespan, we observed no changes in the ^{1}H NMR spectra. Next, to check the effect of the quantity of acid and base separately (*i.e.*, only DCl or only triethylamine), we added another six times the 5-fold excess of DCl and triethylamine. The ^{1}H NMR spectra were recorded after each addition, but the spectra remained again unchanged.

Finally, we examined the behavior of PEG-Bz in D_2O upon seven alternating additions of DCl and triethylamine, so as to simulate the conditions of dissociation and reformation of the acylhydrazone adduct. After each of the fourteen additions, the ^{1}H NMR spectra were recorded. The spectra remained unchanged after the first thirteen additions [alternating additions of DCl (×7) and triethylamine (×6)]. However, upon the seventh addition of triethylamine, the same split in the peak of the benzaldehyde formyl methine as in the seventh acylhydrazone adduct reformation cycle was observed. This suggests that the gradual building up of the triethylamine salt eventually causes the peak split, which may be responsible for the reduced acylhydrazone reversibility. Fig. S12† shows the ^{1}H NMR spectra of the linear PEG-Bz compound in D_2O after seven alternating additions of DCl and triethylamine (methine peak split first observed), and, for comparison, the spectra after one addition of DCl and triethyamine (no methine peak split). We performed another four (total of eleven) alternating additions of the acid and base, and the peak split was preserved and enhanced in all eight further recorded spectra. Finally, we diluted the system twice with D_2O by 50% and then by another 50%, and the peak split disappeared from the first dilution, indicating again that the peak split is due to the salt building up.

Thus, our ^{1}H NMR spectroscopy study indicated that the loss in acylhydrazone reversibility is probably related to a change in the behavior of benzaldehyde. Benzaldehyde is known to readily transform *via* several chemical reactions, including the Cannizzaro reaction (base-induced disproportionation, giving benzoic acid and benzyl alcohol), and autoxidation in air (giving benzoic acid).[33] However, the presently observed change in benzaldehyde behavior is of a physical, rather than chemical, nature. It might be worth investigating the effect of other acid–base pairs on the reversibility of the acylhydrazone cross-links. A greater irreversibility is expected from acid–base pairs leading to salts with a stronger salting out power, such as ammonium sulfate.

Using the same model compounds, we also performed another type of experiment, relevant to the exchange in the acylhydrazone system. This study aimed at better understanding the equilibrium nature of acylhydrazone formation and dissociation, through which, even in the absence of the previously-mentioned benzaldehyde behavior, the conversion to acylhydrazone and its hydrolysis back to acylhydrazide are both always lower than 100%. This experiment involved the gradual hydrolysis of acylhydrazone using DCl ("titration"), with the hydrolysis products being quantitated again by ^{1}H NMR spectroscopy. The molar ratio of the cumulative amount of the DCl titrant to the originally added acylhydrazide (equivalent to the maximum theoretical amount of acylhydrazone that can be formed) was varied from 0.25 to 20.00. The temporal evolution of the reaction was also followed by ^{1}H NMR spectroscopy to make sure that enough time was allowed for equilibration.

The results of this investigation are shown in Fig. 6, again in two forms in the two parts of the figure. Part (a) exhibits the temporal evolution of acylhydrazone concentration in molar percentage units as acylhydrazone concentration changed upon each addition of DCl, whereas part (b) of Fig. 6 plots the equilibrium acylhydrazone concentration against the molar ratio of the cumulative quantity of added DCl divided by the total initial acylhydrazide amount. Fig. 6(a) shows that, upon each addition of DCl (whose moment of addition is marked with a vertical red arrow, and the molar ratio of cumulative DCl to total initial acylhydrazide is indicated above or below the arrow), acylhydrazone concentration instantly drops to its new equilibrium value, suggesting that the kinetics of acylhydrazone hydrolysis is very fast, as already concluded from Fig. 5(a).

Fig. 6(b) plots the variation of equilibrium acylhydrazone concentration against the molar ratio of the cumulative amount of DCl added to the total initial acylhydrazide. As the amount of added DCl increases, the acylhydrazone group concentration decreases, consistent with the expectation that more acid shifts the equilibrium toward the dissociation products of acylhydrazone. Interestingly, we can observe that, at the stoichiometric addition of DCl (ratio = 1.00), the acylhydrazone group concentration has dropped from the initial 91% only down to 64%. To reduce acylhydrazone concentration down to 50%, about twice the stoichiometric (relative to total acylhydrazide) molar amount of DCl is required, whereas a reduction down to 24% and 12%, 10-fold (also the case in Fig. 4) and 20-fold DCl amounts relative to total acylhydrazide, respectively, must be added. Thus, the equilibrium nature of the acylhydrazone dissociation reaction keeps its relative concentration above 10%, despite the fact that a large excess of strong acid has been added.

Thermally-induced self-organization of the APCNs

For gaining a mesoscopic structural understanding of the APCN properties, the self-organization of the T904 dynamic covalent APCNs prepared in aqueous (D_2O) acetate buffer solutions at pD 5.5 and at a 15% w/v polymer concentration was investigated at 25, 40, and 50 °C using small-angle neutron scattering (SANS). Fig. 7 displays the SANS profiles of the APCNs. At the lowest temperature of 25 °C, the SANS profile exhibits a broad shoulder in the q-range of 0.6–0.8 nm^{-1}, indicating the presence of weakly ordered aggregates. Upon raising the temperature to 40 °C, the shoulder transforms into a clear correlation peak that becomes even more pronounced at 50 °C, indicating better ordering of the micellar aggregates. By lowering the temperature back down to 25 °C, the correlation peak reverts to the broad shoulder of the initial SANS profile at 25 °C, suggesting that the temperature-induced ordering is reversible. From the peak position, q_{max}, at the two higher temperatures, 40 and 50 °C, a mean spacing, d (= $2\pi/q_{max}$), of ~8.5 nm between the micelle centers can be calculated. Taking into account the D_2O content and copolymer composition yields an aggregation number, N_{agg}, of ~10–11 (Table 1). This N_{agg} value is approximately one-half of 18–23 determined for the free (non-end-linked) T904 star block copolymer in aqueous solution at the same temperatures and similar polymer concentrations.[34,35] The lower N_{agg} value for the APCN system can be ascribed to the chemical interconnection (end-linking) among the constituting amphiphilic star block copoly-

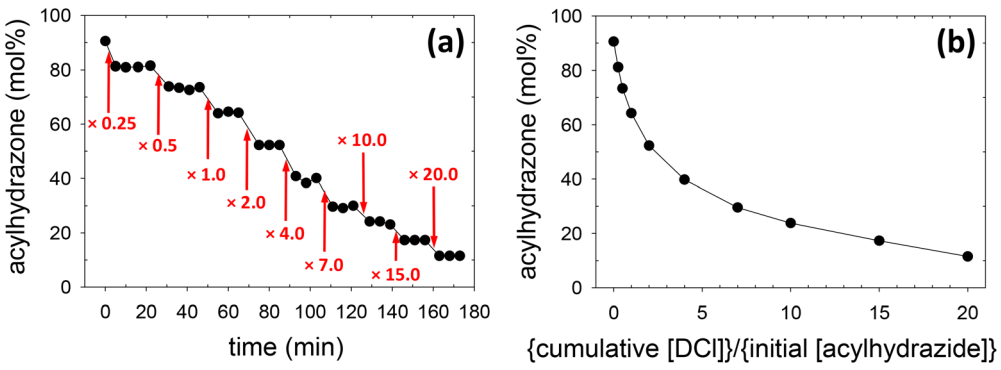

Fig. 6 (a) Temporal evolution of acylhydrazone concentration attained by the addition of DCl at various times marked by arrows, with the cumulative amount of added DCl relative to the initial total acylhydrazide amount also being indicated. (b) Equilibrium isotherm (room temperature) correlating equilibrium acylhydrazone concentration to the cumulative amount of DCl added divided by the initial acylhydrazide concentration.

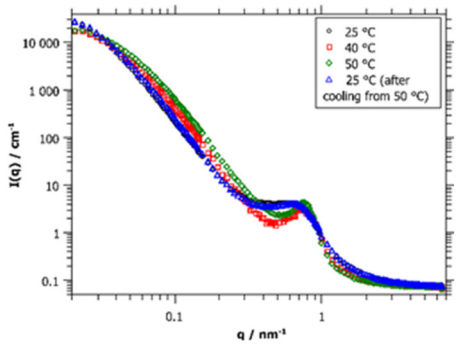

Fig. 7 SANS profiles of the APCNs in the as-prepared state at a 15% w/v total polymer concentration in D_2O buffered at a pD of 5.5, studied at 25, 40, 50 and again back down to 25 °C.

Table 1 Parameters obtained from the SANS analysis of the 15% w/v sample based on the peak position

Temperature (°C)	q_{max} (nm^{-1})	d[a] (nm^{-1})	V_{cell}[b] (nm^3)	φ_{core}[c]	V_{core}[d] (nm^3)	N_{agg}[e]
25 (initial)	—	—	—	0.094	—	—
40	0.734	8.56	627	0.104	65.5	9.7
50	0.749	8.39	591	0.127	75.0	11.1
25 (after cooling from 50 °C)	—	—	—	0.094	—	—

[a] $d = 2\pi/q_{max}$. [b] $V_{cell} = d^3$. [c] φ_{core} = (PPG volume fraction in dry polymer) × (overall polymer volume fraction in swollen gel). PPG volume fraction in dry polymer = 0.626; for this calculation, degrees of polymerization of 17 and 15 were used for the PPG and PEG blocks in each star arm,[34] respectively, whereas the respective PPG and PEG densities were taken as 1.00 and 1.12 g cm^{-3}. Overall polymer volume fraction in swollen gel = (degree of swelling of gel)$^{-1}$; the degrees of swelling were taken from Fig. S14,† appropriately taking into account their temperature dependence. [d] $V_{core} = \varphi_{core} \times V_{cell}$. [e] $N_{agg} = V_{core}/V_{core\ unimer}$; $V_{core\ unimer}$ = 6.55 nm^3; $V_{core\ unimer}$ is the PPG volume in a single star block copolymer, possessing 17 PG units in each of its four arms, again taking the PPG density equal to 1.00 g cm^{-3}.

mers, resulting in lower freedom toward self-assembly, as chain stretching opposes a reduction in interfacial area per chain, the latter of which is the main driving force for micelle formation.

The high q-range of the SANS profiles, including the correlation peak, was described quantitatively by fitting a model of small spherical aggregates composed of hydrated PPG segments that interact *via* a hard-sphere potential (see the ESI† for details). In doing that, we made educated choices for the water content of the PPG core as 45, 40, and 30 vol% at 25, 40, and 50 °C, respectively, based on previous theoretical modeling and SANS experiments on similar amphiphilic linear ABA triblock copolymer systems (Pluronics).[36,37] The main output of this analysis was the radii of the PPG hydrated cores, R_c, which came out to be 2.93, 2.64, and 2.65 nm at 25, 40, and 50 °C (see SANS data fits in Fig. S13† and all fit parameters in Table S3†), respectively. The R_c value of 2.65 nm then translates for the assumed extent of hydration of the core to an aggregation number of ~6 for the hydrophobic cores of T904 molecules (Table S3†), in fair agreement with the determination *via* the mean spacing described above. Our findings are also in good agreement with the R_c value of 2.55 nm obtained previously for free T904 solution using SANS.[38]

Finally, in the low q-range, the SANS profiles exhibit a strong increase in scattering intensity as q decreases, with the intensity leveling off at the lowest measured q values, thereby indicating a finite size of globular structural units. This increase starts earlier for the higher temperatures but reaches about the same intensity at low q, which indicates a superstructure that contains about the same amount of material but becomes more compacted with increasing temperature. The radius of these larger structural units was estimated by applying Guinier's law. Assuming homogeneous spheres, this corresponds to radii of 60, 50, and 45.7 nm at 25, 40, and 50 °C, respectively, *i.e.*, they shrink as the temperature goes up. If one compares the scattering intensity of these large globules with that of the small micelles contained, one finds that each such unit contains about 2600–2800 micelles and this number remains unchanged during the temperature increase (Table S3†), *i.e.*, the large structures shrink but keep the number of hydrophobic micellar units largely unchanged.

Fig. 8 represents the APCN structure derived from the SANS profiles as analyzed above. This includes relatively large globular domains[39] of radii of 45–60 nm, which contain more densely packed micellar aggregates whose hydrated PPG cores have radii of ~3 nm and a mean spacing of ~8.5 nm. The space between the bigger domains can then be assumed to contain some more individual micelles which aggregate outside due to constraints imposed by the polymer co-network structure. The mean spacing between the smaller micellar aggregates is expectedly shorter than the contour length between the centers of two adjacent and interconnected stars of ~21 nm = 64 units × 0.33 nm per unit, due to both microphase separation and chain coiling. Given that the micellar core radii at higher temperatures are 2.65 nm, this implies that the average distance between the surfaces of the cores of two adjacent micelles is 3.2 nm (= 8.5–2 × 2.65). This bridging distance of ~3 nm is consistent with the size of two consecutive hydrophilic blocks of contour length of ~10 nm = 30 units at 0.33 nm per unit, which, in solution are expected to coil to a final size of 30–50% of their contour length.

Upon increasing the temperature, all structural features get increasingly compacted and the whole structure becomes more ordered. The shrinkage can be attributed to the well-known reduced hydration of PEG and PPG with increasing temperature.

Thermally-induced mechanical property enhancement of the APCNs

Finally, the tensile mechanical properties of the T904 dynamic covalent APCNs prepared in aqueous acetate buffer solutions at pH 5.5 and at a 15% w/v polymer concentration were investigated at 25, 40 and 50 °C using mechanical testing in tensile mode, with the samples being stretched while immersed in a thermostated paraffin oil bath, with some samples also tested in air at 20 °C. Table 2 below summarizes these properties, which include the tensile stress at break, σ_{max}, the tensile strain at break, ε_{max}, and Young's modulus, E.

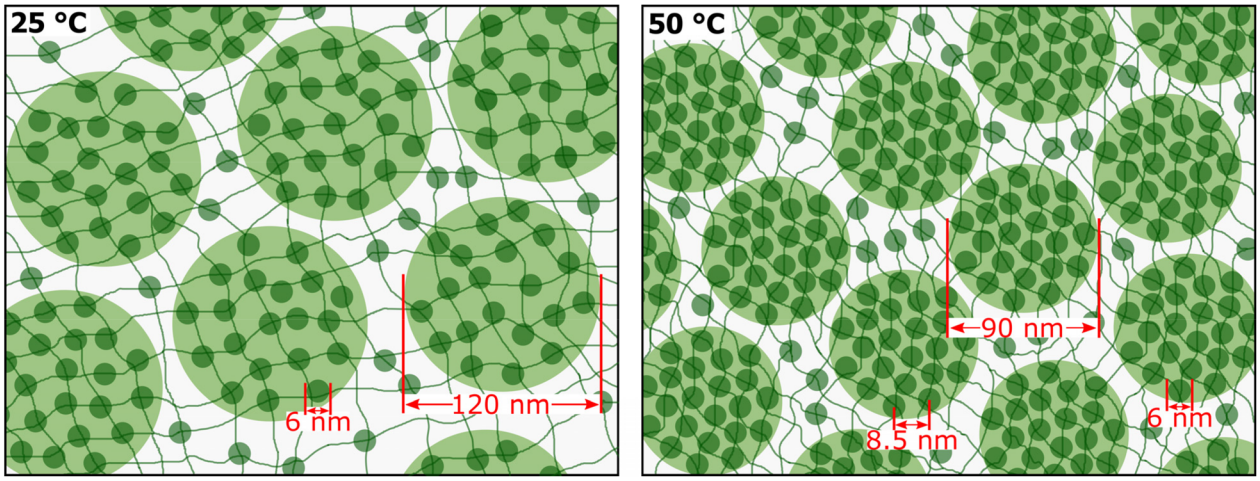

Fig. 8 Structure of self-organized T904 APCNs and its change with increasing temperature.

Table 2 Tensile mechanical properties of the APCNs

T (°C)	σ_{max} (kPa)	ε_{max} (%)	E (kPa)
20	45 ± 1	102 ± 4	51 ± 1
25	41 ± 8	99 ± 17	56 ± 2
40	105 ± 12	127 ± 20	128 ± 3
50	125 ± 40	160 ± 70	145 ± 6

All three mechanical properties at or near room temperature were statistically the same, whether in air or immersed in oil (first two lines in the table), thereby confirming that immersion in oil does not influence the measurements. Increasing the temperature from 25 to 40 and 50 °C led to a significant enhancement in Young's modulus, by 130% at 40 °C and another 15% at 50 °C. Interestingly, these increases in Young's modulus are paralleled by the corresponding enhancements of other mechanical properties. In particular, the thermally induced stiffening resulted in slight increases in stretchability, ~30% with each increase in the temperature, and larger increases in strength, first by 155% when heating from 25 to 40 °C and then another 20% when reaching 50 °C. Although some of the enhancement in the mechanical properties can be attributed to partial shrinking (relative reductions in the swelling degrees of 22% and 25% when the temperature was increased from 25 to 40 °C and 40 to 50 °C, respectively; see Fig. S14 in the ESI†) of the APCN system (unlike our previous APCN systems,[5] the present system did not respond isochorically to a temperature increase), the main part of the increase in both the stress and strain at break as well as Young's modulus can be attributed to the temperature-induced organization of the system as analyzed in the SANS section.

Conclusions

In summary, we have presented the first APCN system, possessing, in addition to amphiphilicity, well-defined star copolymer building blocks end-linked *via* dynamic covalent bonds, whose structural organization was explored using SANS. SANS indicated the formation of weakly-ordered spherical micelles at room temperature which, upon heating up to 40–50 °C, become much more ordered. These small micellar aggregates, in turn, are contained within larger globular domains of ~60 nm, which shrink upon raising the temperature, while keeping the number of micelles contained constant.

This temperature-induced self-organization helped enhance the tensile mechanical properties of the present APCN system, converting it from soft and fragile to hard and tough. Importantly, the dynamic covalent nature of the acylhydrazone cross-links of the developed APCN imparted to it reversibility, self-healing and recyclability with complete recovery of its compressive mechanical properties. Significantly, the successive gel–sol transitions in the present system could be readily followed using simple solution ^{1}H NMR spectroscopy, providing crucial insights as to why the gel–sol cycles cannot be repeated indefinitely. Finally, it might be worth noting that, although the present APCN system based on star block copolymers end-linked *via* dynamic covalent bonds yielded spherical structures, other star-based APCN systems, end-linked *via* permanent chemical bonds, can form lamellae[40,41] or cylinders.[42,43]

Conflicts of interest

There are no conflicts to declare.

Acknowledgements

We gratefully acknowledge the co-funding of this research work by the European Regional Development Fund and the Republic of Cyprus through The Research and Innovation Foundation of Cyprus (Project Number: Excellence/0918/0325). The same organizations are also thanked for funding projects ANAVATHMISI/0609/12 and NEKYP/0308/02, which enabled the

purchase of the rheometer and the NMR spectrometer, respectively, at the University of Cyprus, used in this investigation. Initial funding of this work was provided by the University of Cyprus Research Committee (Research Grant "Hydrogels"). Furthermore, we thankfully acknowledge the SANS beam time and the financial support by Helmholtz-Zentrum Berlin (HZB), Germany. Finally, we thank our colleague Prof. E. Leontidis of the Chemistry Department at the University of Cyprus for kindly providing access to his rheometer used in our experiments.

References

1 *Amphiphilic Polymer Co-Networks: Synthesis, Properties, Modelling and Applications*, ed. C. S. Patrickios, Royal Society of Chemistry, Cambridge, UK, 2020.
2 C. S. Patrickios and K. Matyjaszewski, Amphiphilic polymer co-networks: 32 years old and growing stronger – A perspective, *Polym. Int.*, 2021, **70**, 10–13.
3 A. K. Singh Chandel, B. Nutan, I. H. Raval and S. K. Jewrajka, Self-assembly of partially alkylated dextran-*graft*-poly[(2-dimethylamino)ethyl methacrylate] copolymer facilitating hydrophobic/hydrophilic drug delivery and improving conetwork hydrogel properties, *Biomacromolecules*, 2018, **19**, 1142–1153.
4 S. Kizil and H. B. Sonmez, One-pot fabrication of reusable hybrid sorbents for quick removal of oils from wastewater, *J. Environ. Manage.*, 2020, **261**, 109911.
5 H. Guo, N. Sanson, D. Hourdet and A. Marcellan, Thermoresponsive toughening with crack bifurcation in phase-separated hydrogels under isochoric conditions, *Adv. Mater.*, 2016, **28**, 5857–5864.
6 H. Kamata, Y. Akagi, Y. Kayasuga-Kariya, U.-i. Chung and T. Sakai, "Nonswellable" hydrogel without mechanical hysteresis, *Science*, 2014, **343**, 873–875.
7 S. T. R. Velasquez, D. Jang, P. Jenkins, P. Liu, L. Yang, L. T. J. Korley and N. Bruns, Peptide-reinforced amphiphilic polymer conetworks, *Adv. Funct. Mater.*, 2022, 2207317, DOI: 10.1002/adfm.202207317.
8 M. M. Bomgardner, Making better contact lenses, *Chem. Eng. News*, 2017, **95**(13), 29–33.
9 K. R. McLeod and G. N. Tew, Microphase-separated thiol–ene conetworks from telechelic macromonomers with asymmetric molecular weights, *Macromolecules*, 2017, **50**, 8042–8047.
10 D. E. Apostolides, C. S. Patrickios, T. Sakai, M. Guerre, G. Lopez, B. Améduri, V. Ladmiral, M. Simon, M. Gradzielski, D. Clemens, C. Krumm, J. C. Tiller, B. Ernould and J.-F. Gohy, Near-model amphiphilic polymer conetworks based on four-arm stars of poly(vinylidene fluoride) and poly(ethylene glycol): Synthesis and characterization, *Macromolecules*, 2018, **51**, 2476–2488.
11 T. Stumphauser, G. Kasza, A. Domján, A. Wacha, Z. Varga, Y. Thomann, R. Thomann, B. Pásztoi, T. M. Trötschler, B. Kerscher, R. Mülhaupt and B. Iván, Nanoconfined cross-linked poly(ionic liquid)s with unprecedented selective swelling properties obtained by alkylation in nanophase-separated poly(1-vinylimidazole)-l-poly(tetrahydrofuran) conetworks, *Polymer*, 2020, **12**, 2292.
12 C.-S. Huang, K. Jakubowski, S. Ulrich, S. Yakunin, M. Clerc, C. Toncelli, R. M. Rossi, M. V. Kovalenko and L. F. Boesel, Nano-domains assisted energy transfer in amphiphilic polymer conetworks for wearable luminescent solar concentrators, *Nano Energy*, 2020, **76**, 105039.
13 C.-S. Huang, S. Yakunin, J. Avaro, X. Kang, M. I. Bodnarchuk, M. Liebi, X. Sun, R. M. Rossi, M. V. Kovalenko and L. F. Boesel, Amphiphilic polymer co-network: A versatile matrix for tailoring the photonic energy transfer in wearable energy harvesting devices, *Adv. Energy Mater.*, 2022, **12**, 2200441.
14 S. Ulrich, A. Osypova, G. Panzarasa, R. M. Rossi, N. Bruns and L. F. Boesel, Pyranine-modified amphiphilic polymer conetworks as fluorescent ratiometric pH sensors, *Macromol. Rapid Commun.*, 2019, **40**, 1900360.
15 Z. Mutlu, S. S. Es-haghi and M. Cakmak, Recent trends in advanced contact lenses, *Adv. Healthcare Mater.*, 2019, **8**, 1801390.
16 D. Zeng, A. Ribbe and R. C. Hayward, Anisotropic and interconnected nanoporous materials from randomly end-linked copolymer networks, *Macromolecules*, 2017, **50**, 4668–4676.
17 D. Zeng, A. Ribbe, H. Kim and R. C. Hayward, Stress-induced orientation of cocontinuous nanostructures within randomly end-linked copolymer networks, *ACS Macro Lett.*, 2018, **7**, 828–833.
18 D. Zeng and R. C. Hayward, Effects of randomly end-linked copolymer network parameters on the formation of disordered cocontinuous phases, *Macromolecules*, 2019, **52**, 2642–2650.
19 X.-H. Xu, Y.-X. Li, L. Zhou, N. Liu and Z.-Q. Wu, Precise fabrication of porous polymer frameworks using rigid polyisocyanides as building blocks: from structural regulation to efficient iodine capture, *Chem. Sci.*, 2022, **13**, 1111–1118.
20 H. Zou, Q.-L. Wu, L. Zhou, X.-H. Hou, N. Liu and Z.-Q. Wu, Chiral recognition and resolution based on helical polymers, *Chin. J. Polym. Sci.*, 2021, **39**, 1521–1527.
21 Y.-X. Li, L. Xu, S.-M. Kang, L. Zhou, N. Liu and Z.-Q. Wu, Helicity- and molecular-weight-driven self-sorting and assembly of helical polymers towards two-dimensional smectic architectures and selectively adhesive gels, *Angew. Chem., Int. Ed.*, 2021, **60**, 7174–7179.
22 C. Wang, L. Xu, L. Zhou, N. Liu and Z.-Q. Wu, Asymmetric living supramolecular polymerization: precise fabrication of one-handed helical supramolecular polymers, *Angew. Chem., Int. Ed.*, 2022, **61**, e202207028.
23 C. Michael, D. E. Apostolides, C. S. Patrickios and T. Sakai, Dually-dynamic covalent tetraPEG hydrogels end-linked with boronate ester and acylhydrazone groups, *Soft Matter*, 2022, **18**, 5966–5978.
24 S. J. Rowan, S. J. Cantrill, G. R. L. Cousins, J. K. M. Sanders and J. F. Stoddart, Dynamic covalent chemistry, *Angew. Chem., Int. Ed.*, 2002, **41**, 898–952.

25 Y. Chen, D. Diaz-Dussan, D. Wu, W. Wang, Y.-Y. Peng, A. Benozir Asha, D. G. Hall, K. Ishihara and R. Narain, Bioinspired self-healing hydrogel based on benzoxaborolecatechol dynamic covalent chemistry for 3D cell encapsulation, *ACS Macro Lett.*, 2018, **7**, 904–908.
26 D. E. Apostolides and C. S. Patrickios, Dynamic covalent polymer hydrogels and organogels crosslinked through acylhydrazone bonds: Synthesis, characterization and applications, *Polym. Int.*, 2018, **67**, 627–649.
27 G. Hild, Model networks based on 'endlinking' processes: Synthesis, structure and properties, *Prog. Polym. Sci.*, 1998, **23**, 1019–1149.
28 P. Wang, G. Deng, L. Zhou, Z. Li and Y. Chen, Ultrastretchable, self-healable hydrogels based on dynamic covalent bonding and triblock copolymer micellization, *ACS Macro Lett.*, 2017, **6**, 881–886.
29 D. E. Apostolides, T. Sakai and C. S. Patrickios, Dynamic covalent star poly(ethylene glycol) model hydrogels: A new platform for mechanically robust, multifunctional materials, *Macromolecules*, 2017, **50**, 2155–2164.
30 G. Deng, C. M. Tang, F. Y. Li, H. F. Jiang and Y. M. Chen, Covalent cross-linked polymer gels with reversible sol-gel transition and self-healing properties, *Macromolecules*, 2010, **43**, 1191–1194.
31 J. Kalia and R. T. Raines, Hydrolytic stability of hydrazones and oximes, *Angew. Chem., Int. Ed.*, 2008, **47**, 7523–7526.
32 C. Bunk, L. Löser, L. Fribiczer, H. Komber, L. Jakisch, R. Scholz, B. Voit, S. Seiffert, K. Saalwächter, M. Lang and F. Böhme, Amphiphilic model networks based on PEG and PCL tetra-arm star polymers with complementary reactivity, *Macromolecules*, 2022, **55**, 6573–6589.
33 M. Sankar, E. Nowicka, E. Carter, D. M. Murphy, D. W. Knight, D. Bethell and G. J. Hutchings, The benzaldehyde oxidation paradox explained by the interception of peroxy radical by benzyl alcohol, *Nat. Commun.*, 2014, **5**, 3332.
34 Y. Kadam, K. Singh, D. G. Marangoni, J. H. Ma, V. K. Aswal and P. Bahadur, Induced micellization and micellar transition in aqueous solution of nonlinear block co-polymer tetronic T904, *J. Colloid Interface Sci.*, 2010, **351**, 449–456.
35 G. González-Gaitano, C. Müller, A. Radulescu and C. A. Dreiss, Modulating the self-assembly of amphiphilic X-shaped block copolymers with cyclodextrins: Structure and mechanisms, *Langmuir*, 2015, **31**, 4096–4105.
36 M. Svensson, P. Alexandridis and P. Linse, Phase behavior and microstructure in binary block copolymer/selective solvent systems: Experiments and theory, *Macromolecules*, 1999, **32**, 637–645.
37 L. Yang, P. Alexandridis, D. C. Steytler, M. J. Kositza and J. F. Holzwarth, Small-angle neutron scattering investigation of the temperature-dependent aggregation behavior of the block copolymer pluronic L64 in aqueous solution, *Langmuir*, 2000, **16**, 8555–8561.
38 R. Ganguly, Y. Kadam, N. Choudhury, V. K. Aswal and P. Bahadur, Growth and interaction of the Tetronic 904 micelles in aqueous alkaline solutions, *J. Phys. Chem. B*, 2011, **115**, 3425–3433.
39 Y. Hu, L. Barbier, Z. Li, X. Ji, H. Le Blay, D. Hourdet, N. Sanson, J. W. Y. Lam, A. Marcellan and B. Z. Tang, Hydrophilicity-hydrophobicity transformation, thermo-responsive morphomechanics, and crack multifurcation revealed by AIEgens in mechanically strong hydrogels, *Adv. Mater.*, 2021, **33**, 2101500.
40 E. J. Kepola, E. Loizou, C. S. Patrickios, E. Leontidis, C. Voutouri, T. Stylianopoulos, R. Schweins, M. Gradzielski, C. Krumm, J. C. Tiller, M. Kushnir and C. Wesdemiotis, Amphiphilic polymer conetworks based on end-linked "core-first" star block copolymers: Structure formation with long-range order, *ACS Macro Lett.*, 2015, **4**, 1163–1168.
41 T. Hiroi, S. Kondo, T. Sakai, E. P. Gilbert, Y.-S. Han, T.-H. Kim and M. Shibayama, Fabrication and structural characterization of module-assembled amphiphilic conetwork gels, *Macromolecules*, 2016, **49**, 4940–4947.
42 K. Mortensen and M. Annaka, Structural study of four-armed amphiphilic star-block copolymers: Pristine and end-linked Tetronic T1307, *ACS Macro Lett.*, 2016, **5**, 224–228.
43 K. Mortensen and M. Annaka, Stretching PEO – PPO type of star block copolymer gels: Rheology and small-angle scattering, *ACS Macro Lett.*, 2018, **7**, 1438–1442.